Journal of Materials Chemistry A

COMMUNICATION

View Article Online
View Journal | View Issue

Cite this: J. Mater. Chem. A, 2018, 6, 9846

Received 5th January 2018
Accepted 17th April 2018

DOI: 10.1039/c8ta00153g

rsc.li/materials-a

Highly interconnected hollow graphene nanospheres as an advanced high energy and high power cathode for sodium metal batteries†

Ranjith Thangavel, ‡[a] Aravindaraj G. Kannan, ‡[b] Rubha Ponraj,[b] Xueliang Sun,[c] Dong-Won Kim *[b] and Yun-Sung Lee *[a]

Developing sodium based energy storage systems that retain high energy density at high power along with stable cycling is of paramount importance to meet the energy demands of next generation applications. This requires the development of electrodes beyond the conventional intercalation-based chemistry to overcome the sluggish diffusion-limited reaction kinetics and limited cycle life. Herein, we report a rationally designed hollow graphene nanosphere (HGS) cathode, which utilizes non-destructive, ultra-fast surface redox reactions at oxygen functional groups and delivers a discharge capacity of ~155 mA h g^{-1} (0.1 A g^{-1}) corresponding to a high energy of ~415 W h kg^{-1} and retains ~88 W h kg^{-1} of energy at a remarkable specific power of ~84 kW kg^{-1} (40 A g^{-1}), which are beyond the capabilities of intercalation-based electrodes. Moreover, the achieved cycling performance (86% capacity retention after 50 000 cycles at 10 A g^{-1}) is the most stable cathode performance reported so far. The rationally designed sodium metal battery full cells with a sodium metal deposited aluminium current collector anode and the HGS cathode showed a similar sodium ion storage performance with high capacity, good rate capability, and stability. We certainly believe that the current research could direct the future research development towards transition metal-free, ultra-high power and super stable cathodes for sodium energy storage devices.

The ever increasing global energy demand and its impact on the environment have led to the rapid development of renewable energy sources such as solar and wind, which are highly intermittent in nature and require cost-effective energy storage systems with faster reaction kinetics, high energy density and ultra-long cycle life.[1,2] Although supercapacitors can deliver high power and long cycle life, their low energy density impedes their applications in such systems. Rechargeable sodium based storage devices such as sodium ion batteries (NIBs) and sodium metal batteries could be a promising alternative due to the abundant availability and low cost of sodium metal along with their well-known reaction chemistry, which is similar to that of lithium ion batteries.[3,4] Although significant progress has been made in the performance of sodium storage devices through advancements in cathodes, anodes, sodium metal hosts and electrolytes, they still do not satisfy the needs of next generation applications. The crucial problem that remains unsolved is the sluggish reaction kinetics of NIBs due to the larger ionic size of sodium along with the diffusion-limited intercalation/extraction of sodium ions within the sodium hosts.[5,6] Also, a large structural change in the electrode during repeated Na^+ insertion/extraction lowers the capacity and cycle life.[7,8] Surface driven sodium charge storage utilizing transition metal-free carbonaceous cathodes could overcome the sluggish diffusion and intercalation kinetics.[9,10] Energized by metal-free non-intercalation chemistries, ultra-high energy and power densities can be achieved utilizing reversible sodium ion storage in carboxylic groups present in carbonaceous materials.[11] Recently, functional group-enriched graphene-based cathodes such as graphene platelets, nanocellular foams, and folded graphene have been demonstrated as metal-free high power cathodes for sodium based energy storage systems.[11–13] Yet, the specific power output and capacity retention at higher currents are not appealing and need further improvements. Moreover, the conventional planar graphene sheets are prone to re-stacking and form intrinsic corrugations during processing, resulting in a reduced active surface area and decreased ion accessibility.[14] To mitigate these issues, the rational design of graphene nanosheets into advanced multifunctional structures that effectively utilize their surface functional groups is critical. On the other hand, hollow architectures are well known to improve the surface utilization of any active material thereby enhancing the rate capability and stability.[15–17] Therefore,

[a]Faculty of Applied Chemical Engineering, Chonnam National University, Gwang-ju 500-757, Republic of Korea. E-mail: leeys@chonnam.ac.kr

[b]Department of Chemical Engineering, Hanyang University, Seoul 04763, Republic of Korea. E-mail: dongwonkim@hanyang.ac.kr

[c]Department of Mechanical and Materials Engineering, University of Western Ontario, London-N6A 5B9, Canada

† Electronic supplementary information (ESI) available. See DOI: 10.1039/c8ta00153g

‡ Both authors have equal contribution.

assembling graphene nanosheets into such hollow structures could enormously boost the output performance of sodium ion based energy storage devices. Additionally, such metal-free cathodes require sodium containing low voltage anodes or sodium metal itself as the anode, and sodium full cells based on metal-free cathodes have not been widely investigated so far.

Herein, we demonstrate for the first time the use of highly interconnected hollow graphene spheres (HGSs) as a high-performance cathode for sodium energy storage systems with battery-like energy density and capacitor-like power and lifetime. HGSs were prepared by assembling graphene oxide (GO) onto amino-functionalized silica sphere templates through electrostatic interactions, followed by reduction and template removal. The HGS cathode can reversibly store sodium ions through surface faradaic reactions with carboxylic groups (elucidated using X-ray photoelectron spectroscopy (XPS) and transmission electron microscopy (TEM)) and deliver a capacity of $\sim$155 mA h g^{-1} in a half-cell configuration. The HGS electrodes exhibited a high energy density of $\sim$410 W h kg^{-1} and an ultra-high power of $\sim$84 kW kg^{-1}, which are beyond the capabilities of intercalation-based compounds. In addition, ultra-stable performance for 50 000 cycles has been documented for the first time, outperforming the stability of previously reported sodium ion cathode materials and approaching the cycling performance of capacitors. The novelty of the current work lies in the development of high energy and high power sodium cathodes with ultra-long stability by assembling graphene nanosheets into a continuous 3-dimensional structure. This effectively prevented the re-stacking of graphene sheets during processing thereby exposing the surface functional groups. In addition, a sodium metal full cell based on the metal-free HGS cathode is demonstrated in this work. Remarkably, when full cells are assembled with the HGS cathode and a sodium deposited aluminum current collector anode, the sodium metal batteries can perform extremely well in a similar fashion with high capacity (131 mA h g^{-1} at 0.2 A g^{-1}) and rate capability. The current research approach may shed some light on the development of next generation ultra-stable sodium energy storage systems with a blend of high energy, ultra-high power and durability.

To effectively utilize the superior properties of graphene nanosheets, 2-dimensional graphene sheets were assembled into highly interconnected 3-D structures using a sacrificial template method as depicted in Scheme 1. An amino-functionalized silica sphere template was prepared using a two-step sol–gel method, where tetraethyl orthosilicate was used as a precursor for silica synthesis followed by surface modification using (3-aminopropyltriethoxy)silane. In the first step of HGS preparation, yolk–shell structured GO wrapped amino-functionalized silica sphere templates were prepared by utilizing the electrostatic interaction between the positively charged amino groups present on the functionalized silica surface and the negatively charged oxygen functional groups on GO. Upon thermal reduction (at 700 °C in an Ar atmosphere) in the subsequent step, reduced graphene oxide (rGO) covered templates were obtained. Finally, the template was etched using hydrofluoric acid to obtain HGSs (more detailed experimental conditions are given in the ESI†). The size of the spherical template was found to be in the range of 230–280 nm (ESI, Fig. S1a†). The uniform coverage of the spherical template with rGO was clearly evident from the scanning electron microscopy (SEM) and TEM images (Fig. S1b,† 1a and b, respectively). Such a uniform coverage was possible due to the electrostatic interaction between the GO sheets and the template. Although a slight contraction occurred during the etching step, a stable hollow structure was obtained without the support of the template owing to the high mechanical strength of rGO.[18–20] Another notable feature is the highly interconnected nature of

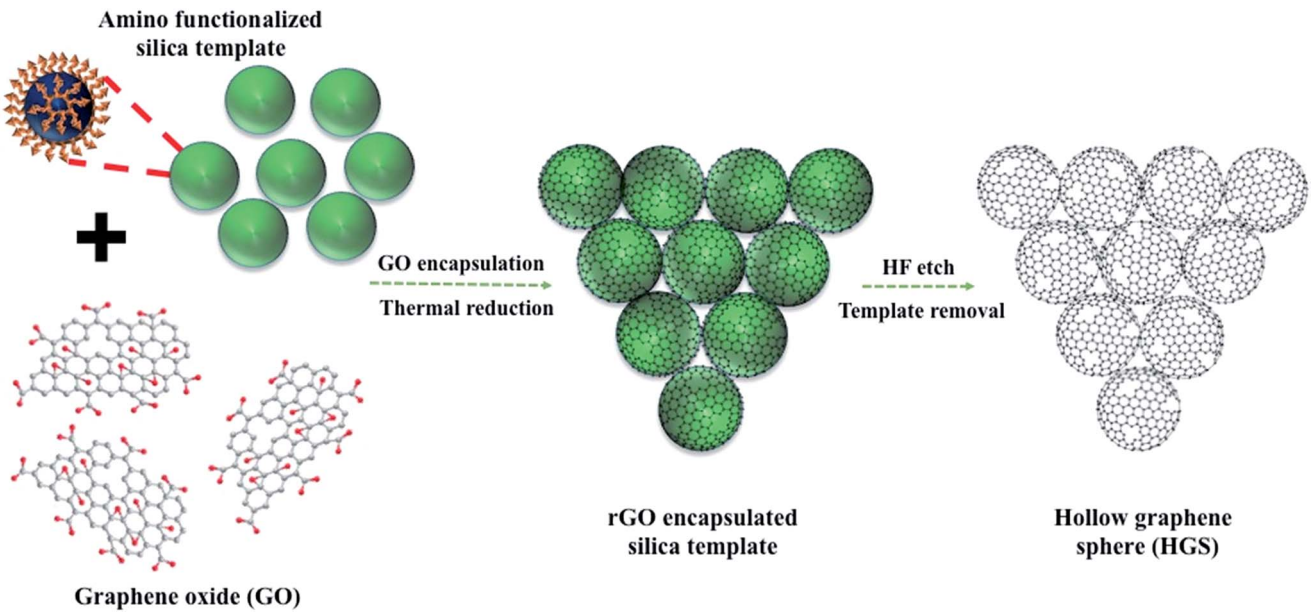

Scheme 1 Schematic illustration of the preparation of HGSs using a template method.

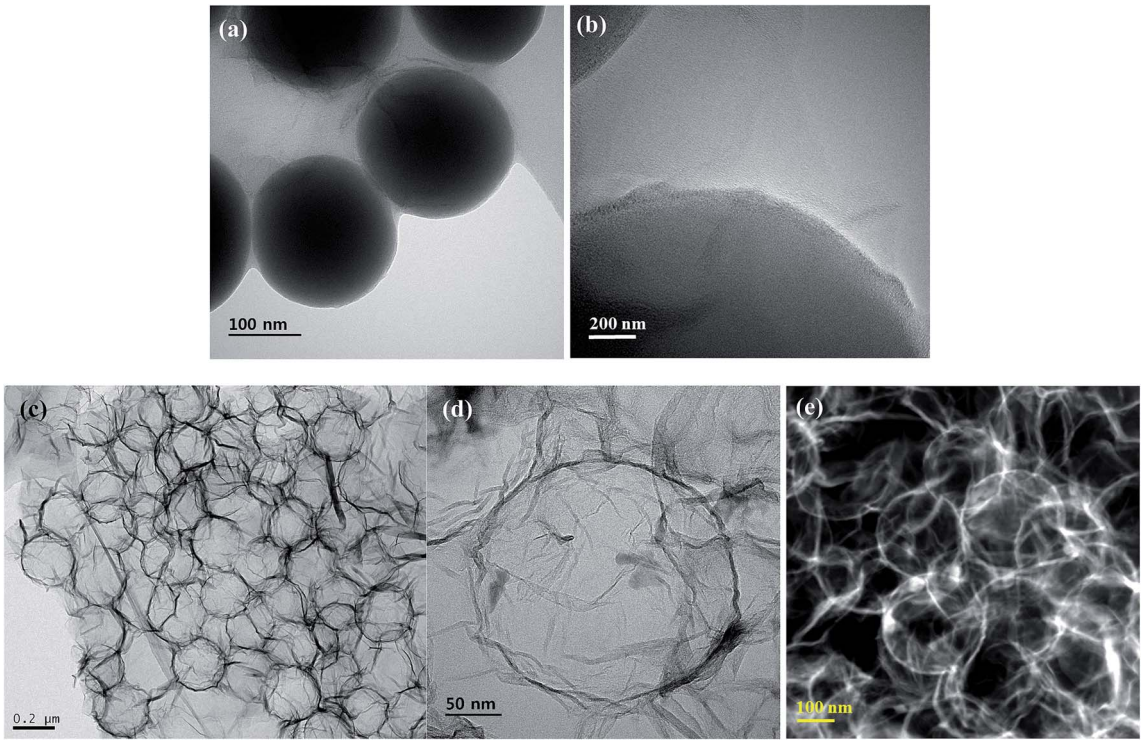

Fig. 1 (a) and (b) TEM images of the rGO encapsulated SiO_2 template, and (c)–(e) TEM images of HGSs.

HGSs as clearly evident from the SEM and TEM images in Fig. S1c and d† and 1c–e, respectively, which is crucial to establish continuous electron transfer between neighboring hollow spheres. Such connected structures were possible due to the 2-dimensional nature of GO, where the larger dimensions of GO enabled it to wrap individual amino-functionalized silica spheres as well as connect the neighboring spheres.[21] More importantly, the assembly of graphene sheets into 3-D architectures confined them from restacking during the thermal treatment step thereby exposing more surface functional groups.[22,23] The ratio between the template and GO is essential to achieve a well interconnected nanosphere morphology. With a higher silica template ratio, the interconnected nature is not retained while with a higher GO ratio, wastage of GO is noted during the centrifugation step.

The chemical composition of HGSs as determined from XPS (Fig. S2a†) was found to be 85.67 at% and 14.31 at% of carbon and oxygen, respectively. In contrast, the amount of carbon/oxygen in GO and rGO (prepared as a control sample using the same procedure as HGSs except using the template) was determined to be 68.88/31.12 at% (not given) and 86.23/13.77 at% (Fig. S2c†), respectively, indicating that GO was substantially reduced during the thermal treatment step. This result shows that the chemical compositions of HGS and rGO control samples are similar and any possible difference in their electrochemical performance would result from their morphological differences. In addition, no silica peaks were detected in the XPS spectrum confirming the complete removal of silica templates. Additionally, peaks due to the nitrogen heteroatom were also not detected in the XPS survey spectrum which could be below the detection limit. The Raman spectrum of HGSs (Fig. S2b†) further confirms the reduction of GO during the thermal treatment step, where the I_D/I_G ratio was determined to be 0.87 and 1.04 for GO and HGSs, respectively.[24] The increase in I_D/I_G after GO reduction is a common phenomenon and is attributed to reduction in the average size of sp^2 domains, in which new sp^2 domains have smaller sizes than the graphitic domains in GO. Although HGSs have more defect-free sp^2 carbon after reduction, the carbon from the smaller graphitic domain than in GO leads to structural defects in HGSs. Additionally, the increase in graphene edges after GO reduction could lead to an increase in the I_D/I_G ratio. The BET surface area of HGSs is $\sim$340 $m^2\ g^{-1}$ and their pore volume is 0.71 $cm^3\ g^{-1}$, indicating the highly porous nature of HGSs (Fig. S3†), while the rGO prepared without a silica template has a BET surface area of $\sim$251 $m^2\ g^{-1}$with a pore volume of 0.22 $cm^3\ g^{-1}$. The highly mesoporous nature of HGSs with wider pore volume can offer a large number of electrolyte reservoir sites, and provide channels for fast sodium ion transport, favoring high rate and stability.

A coin-type cell configuration was used to evaluate the electrochemical performance of HGSs as a cathode by coupling with commercial sodium metal anodes. The cyclic voltammetry (CV) curves (Fig. 2a) show the presence of a broad redox peak between 1.5–4.2 V (clearly visible at high scan rates), and are not in a perfect rectangular shape. The absence of a perfect rectangular shape and the presence of broad redox peaks indicate reversible sodium uptake and release in HGSs through faradaic reactions.[25,26] The large number of oxygen containing carboxyl functional groups are the active sites for sodium storage.

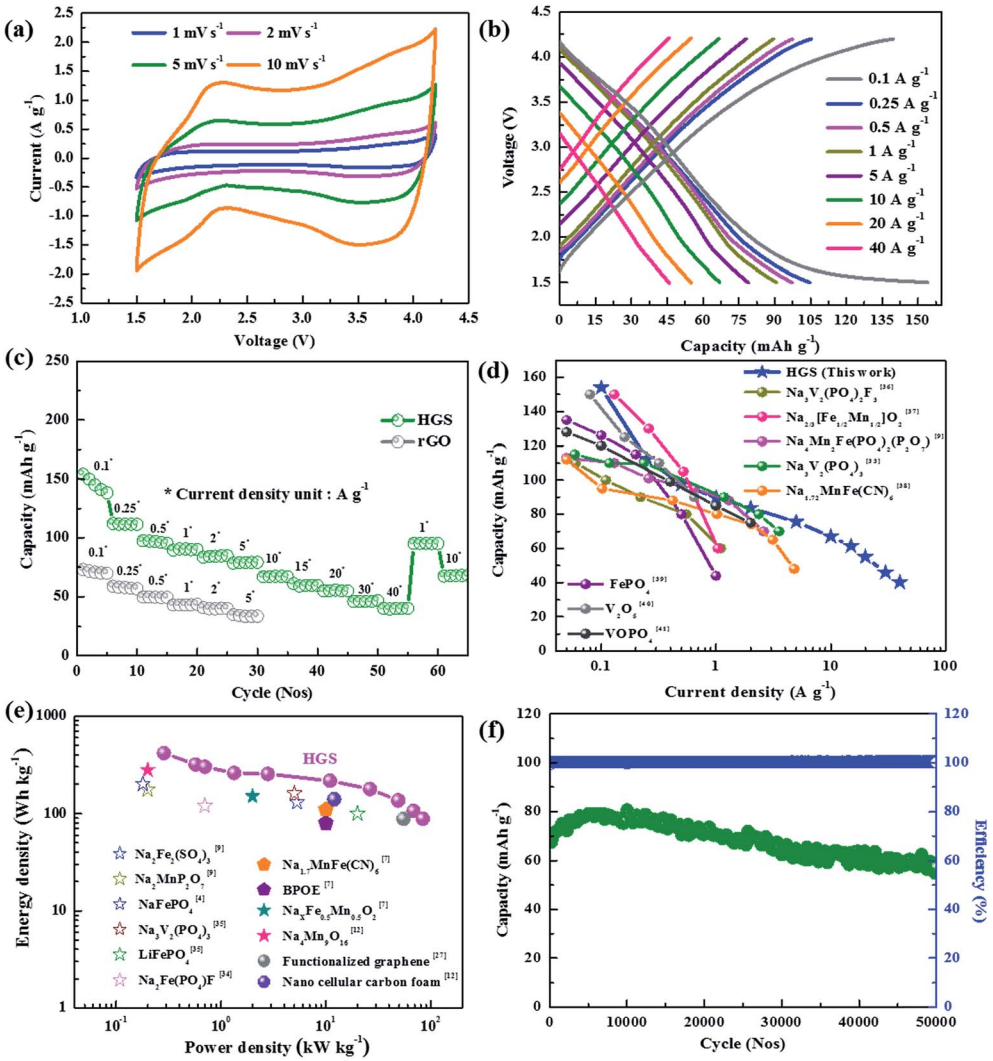

Fig. 2 (a) Cyclic voltammograms of HGSs in NIBs, (b) charge/discharge profile of HGSs in NIBs, (c) rate performance comparison of HGS and rGO control samples, (d) rate capability comparison of HGS and other reported cathodes, (e) Ragone plot of HGSs and comparison with other reported cathodes, and (f) long term cycling stability of HGSs at 10 A g^{-1}.

Moreover, the current response with the increase in the scan rate in HGSs was highly linear (Fig. S4†), indicating a surface mediated ion storage kinetics rather than a diffusion-limited bulk reaction.[11,27] Therefore, the sodium ion storage chemistry in HGSs could be attributed to the redox reaction between sodium ions and oxygen containing surface moieties (discussed below). The applicability of HGSs towards NIBs was further evaluated by galvanostatic charge–discharge (CD) cycling between 1.5 and 4.2 V. The representative CD curves of HGSs obtained at different current densities are given in Fig. 2b. The CD curves at all current rates showed no apparent voltage plateau and delivered a high capacity of ~155 mA h g^{-1} at 0.1 A g^{-1} with an average voltage of ~2.8 V (*vs.* Na), and an initial stabilization was noted. The lack of a plateau indicates that the reaction is limited to the surface. The obtained capacity is much higher than the theoretical capacity of several reported layered oxide, NASICON, pyrophosphate and metal phosphate cathodes for sodium ion batteries.[28,29] In addition, HGSs exhibited a remarkable rate capability, functioning efficiently even at an extremely high current of 40 A g^{-1} and delivered a discharge capacity of ~40 mA h g^{-1}. Even after the high rate measurements, about 100% of the initial capacity was recovered when the current density was reversed back to 1 A g^{-1} and then to 10 A g^{-1} (Fig. 2c). Meanwhile, unassembled rGO sheets delivered a much lower discharge capacity of ~70 mA h g^{-1} at 0.1 A g^{-1} (Fig. S5†) and also exhibited poor rate performance (Fig. 2c). These results demonstrate the superiority of HGSs over rGO sheets even though their chemical compositions and surface functional moieties are similar. The high capacity and excellent rate performance of HGSs could be attributed to their favorable hollow nanosphere architecture, which facilitated maximum utilization of active sites in graphene sheets and the highly connected graphene network enabled a continuous electron transfer pathway to the current collector.[30,31] On the contrary, rGO nanosheets re-stacked in the control sample during the thermal treatment step, resulting in a reduced active surface

area and ion accessibility. To further demonstrate the superior rate performance of HGSs, the discharge capacity of HGSs at various current rates is compared with several previously reported cathodes (Fig. 2d). The high current behavior of HGSs surpassed the performance of conventional transition metal based intercalation cathodes and even outperformed the fast sodium ion conducting NASICON-structured cathodes. Although cathodes such as $Na_3V_2(PO_4)_2F_3$ and $Na_{2/3}[Fe_{1/2}Mn_{1/2}]O_2$ exhibited comparable capacities at low current rates, their performances at higher current rates were inferior to HGSs due to the diffusion-limited reaction kinetics of these electrodes.[32–34] On the contrary, the HGS cathode benefitted from the faster surface-only reaction of sodium ions with the surface oxygen functional groups and delivered a higher capacity than metal containing electrodes.[35–43]

The superiority of HGSs is further demonstrated from the Ragone plots presented in Fig. 2e. The HGS electrode delivered a high energy density of ~416 W h kg^{-1} at a specific power of ~0.29 kW kg^{-1}. Remarkably, it could maintain a high energy of ~88 W h kg^{-1} when the specific power was increased by a factor of ~290 (*i.e.*, 84 kW kg^{-1}). This shows that the HGS electrode retained energy densities similar to that of NIBs while operating at capacitor-like power densities. Moreover, the attained high energy density and high energy retention at high power are remarkably better than those of the conventional layered oxide, NASICON, pyrophosphate, sulfate, fluorophosphate, Prussian blue and organic cathodes.[3,4,10] Such an excellent performance is attributed to the favorable hollow nanosphere architecture with a highly interconnected architecture that enabled effective utilization of surface functional moieties in graphene sheets through a faster surface-only sodium ion storage mechanism.

Long term cyclability at high current rates is another critical parameter that determines the practical applicability of high power energy storage devices. When HGSs were cycled at 10 A g^{-1}, an initial discharge capacity of ~70 mA h g^{-1} was achieved and the capacity gradually increased to 80 mA h g^{-1} after 5000 cycles, which could be attributed to the activation process in the porous materials. The HGS cathode remarkably exhibited capacitor-like cycling stability with ~86% of its initial capacity maintained after 50 000 cycles, while maintaining ~100% coulombic efficiency throughout cycling (Fig. 2f). The capacity loss was calculated to be ~0.28% per 1000 cycles, the lowest ever documented for any cathode. Such a highly reversible sodium charge storage mechanism elevates HGSs as a promising ultra-stable high power cathode. Generally, the conventional intercalation type cathodes are stable for only a few hundred cycles due to the continuous dissolution of transition metals in the electrolyte resulting in structural instability and even the state-of-the-art NASICON-type cathodes are stable for only a few thousand cycles.[32–35] Additionally, the stability of previously reported graphene cathodes in NIBs is still in the range of a few thousand cycles. In comparison, the cycling performance of HGSs is several orders higher than those of other reported cathodes for sodium ion batteries. To understand this extremely durable, capacitor-like cycling performance of HGSs, post-mortem *ex situ* analysis of the HGS electrode after 50 000 cycles was carried out. TEM images (Fig. S6†) of the HGS electrode after 50 000 cycles demonstrate that the hollow nanosphere morphology was well preserved even after ultra-long cycling at a high current rate indicating non-destructive sodium ion storage on the surface functional groups of HGSs.

To elucidate the sodium storage mechanism in HGSs, TEM and XPS analyses were carried out. TEM images (Fig. 3a and b) of HGSs show no morphology change in HGSs at the discharged state (1.5 V *vs.* Na) and TEM-energy dispersive X-ray spectroscopy (EDS) mapping of the HGS electrode (Fig. 3c) at the discharged state (1.5 V *vs.* Na) clearly shows uniform distribution of carbon, oxygen and sodium on hollow sphere structures. Interestingly, sodium distribution is predominantly present on the oxygen sites, which demonstrates the active role of oxygen functional groups in sodium ion storage. This claim is further validated by the high-resolution XPS spectra presented in Fig. 3d and e. The deconvoluted C1s XPS spectrum of HGSs before cycling shows the presence of peaks at 284.5 eV, 285.6 eV and 287.8 eV, which are attributed to C–C, C–O and C=O groups, respectively. After cycling at the discharged state (1.5 V *vs.* Na), the intensity of the C=O peak decreased drastically and a corresponding increase in the C–O peak was noted. This behavior was reversed to the original state upon charging (4.2 V *vs.* Na), indicating the reversible reaction at C=O sites as represented in Fig. 3d. Moreover, the O1s XPS spectrum (Fig. 3e) of HGSs before cycling was deconvoluted into two peaks at 530.2 eV and 532.7 eV, which could be attributed to double-bonded and single-bonded oxygen, respectively. The notable differences upon sodiation of the HGS electrode are the appearance of a broad peak centered at 538 eV representing the sodium auger peak and the diminished peak corresponding to double-bonded oxygen. After charging, the peak corresponding to the sodium auger contribution disappeared and the intensity of double-bonded oxygen was restored. From these XPS results, we can elucidate the reaction mechanism as depicted in Fig. 3f, where reversible sodium storage occurs at C=O sites present on the HGS surface through the transformation of the carbon–oxygen double bond into the carbon–oxygen single bond.[11,44,45] The reduction temperature is a key parameter that determines the amount of oxygen-containing functional groups and the electronic conductivity of HGSs and therefore, the effect of reduction temperature on the performance of HGSs was also evaluated. Increasing the reduction temperature from 600 °C to 900 °C decreased the oxygen functionalities over HGSs, which can be evidenced from the XPS spectra in Fig. S7a.† The increase in the reduction temperature significantly decreased the carbonyl groups (C=O) at 287.8 eV, and partially decreased the epoxide (C–O) peak at 285.6e eV, thereby minimizing the active redox sites (Fig. S7b†). In addition, the C/O ratio drastically increased from 4.02 to 11.82 when the reduction temperature was increased from 600 °C to 900 °C. A higher C/O ratio in general indicates better electronic conductivity. HGSs reduced at 800 °C and 900 °C delivered discharge capacities of ~119 and ~94 mA h g^{-1} at 0.1 A g^{-1}, respectively. In contrast, HGSs reduced at 700 °C and 600 °C delivered discharge capacities of ~155 mA h g^{-1} and 135 mA h g^{-1}, respectively (Fig. S7c†). The decrease in redox-active oxygen functionalities over the HGS surface on reduction at higher temperature decreased the

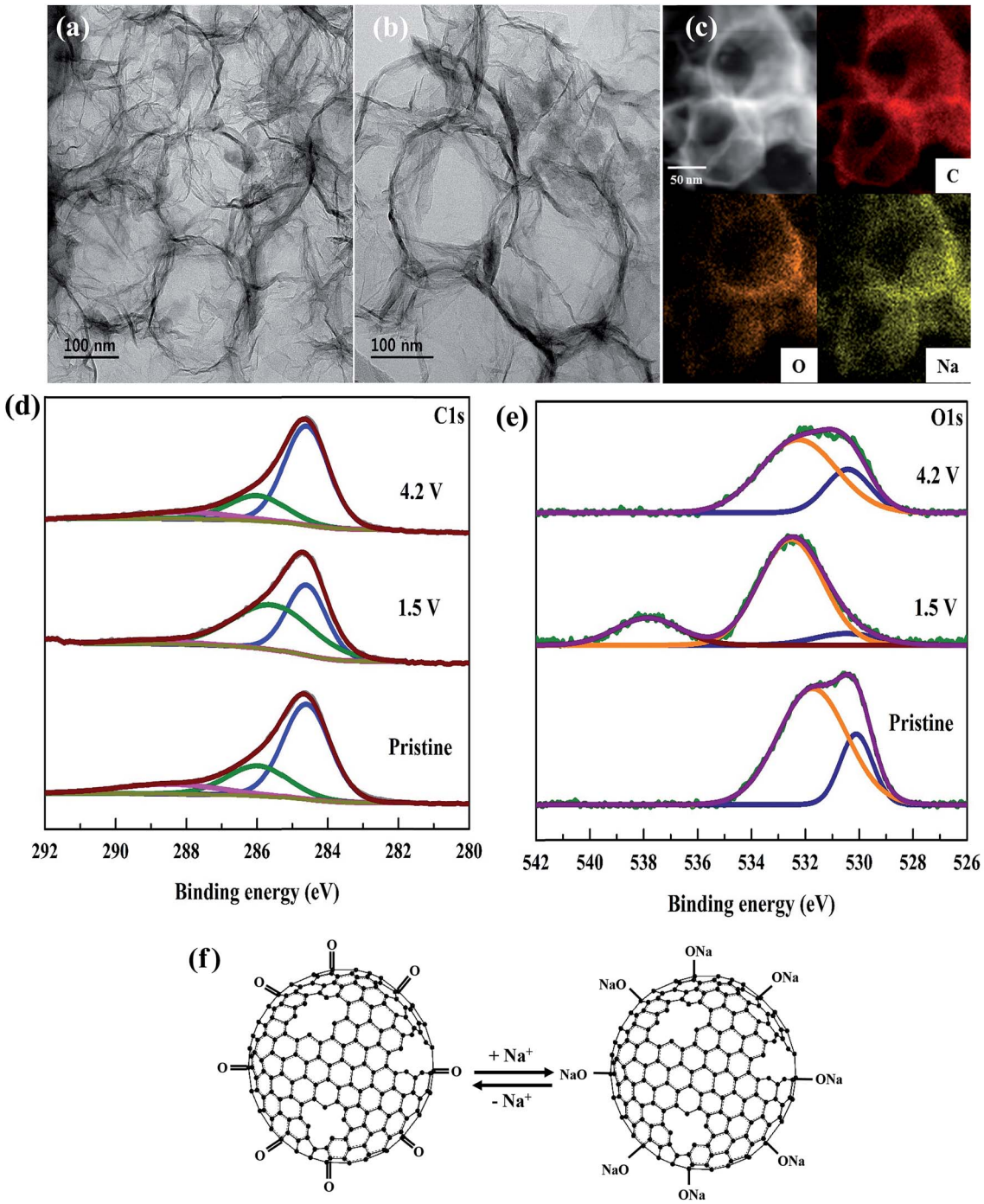

Fig. 3 Characterization of HGSs at the discharged state (1.5 V *vs.* Na): (a) and (b) TEM images, (c) EDS maps, (d) deconvoluted C1s XPS spectrum, (e) deconvoluted O1s XPS spectrum, and (f) schematic of the storage mechanism of HGSs.

capacity, whereas the electronic conductivity played a key role when the reduction temperature was decreased to 600 °C. Therefore, the optimum reduction temperature was found to be 700 °C.

Prompted by the above results, it is expected that the HGSs can be a promising candidate for sodium full-cells. HGSs with no sodium, a low voltage and a sodium containing anode are essential for full-cell construction. Recent studies show the possibility of sodium metal itself serving as a high performance and long life metal anode if engineered efficiently in a host.[46–48] Inspired by the recent finding by C. L. Pint *et al.*, which demonstrated a carbon coated aluminium current collector as a high performance sodium metal host, we constructed a sodium metal battery with the HGS cathode and a sodium metal deposited carbon coated aluminum current collector anode.[49] The full-cell can perform extremely well, with similar performance delivering a discharge capacity of ~131 mA h g^{-1} at 0.2 A g^{-1} and the charge–discharge profile shows a similar

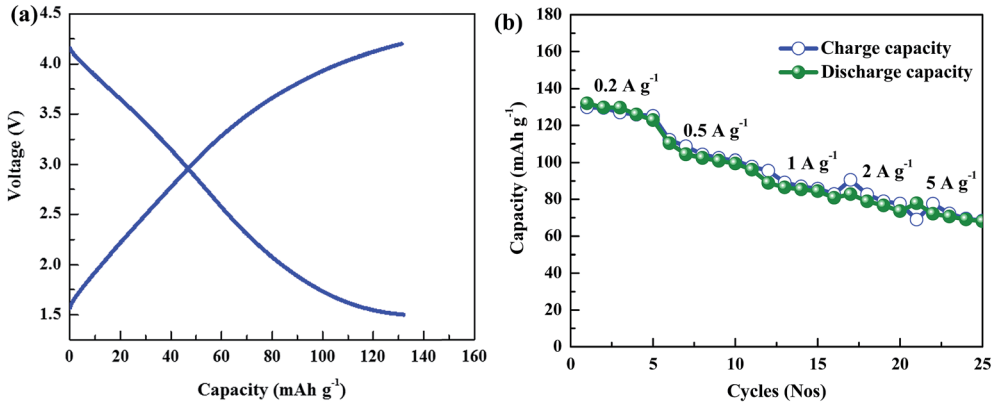

Fig. 4 (a) CD curves of the sodium metal full-cell at 0.2 A g^{-1}, and (b) the rate performance of the full-cell.

pattern (Fig. 4a). The full-cell can deliver almost a similar capacity even after the 50th cycle. Even at a high current of 5 A g^{-1}, a discharge capacity of ~73 mA h g^{-1} has been achieved (Fig. 4b), equivalent to half-cell performance which is still beyond the performance of intercalation type cathodes.[5] At a higher current, the full-cell delivered a poor capacity compared to the half-cell and this could be attributed to the inability of the sodium metal anode to function under high current conditions.[46–50] Further research towards designing an efficient sodium metal host and electrolyte composition can increase the full-cell performance in future and could result in high performance sodium metal batteries.

Conclusions

In summary, we demonstrated that the rational design of graphene nanosheets into a hollow sphere architecture enabled them to be a high energy and high power cathode material with ultra-long stability for advanced sodium energy storage devices. Driven by ultra-fast and highly reversible surface-only sodium ion storage, the storage kinetics are several orders faster than those of the conventional intercalation type cathodes used in sodium ion batteries. Favored by non-destructive sodium ion storage in a 3D architecture by utilizing surface oxygen functional groups, a high capacity, high energy retention and ultra-high specific power were achieved along with superior stability. The rationally designed sodium metal full-cell battery also performed extremely well with high capacity, rate capability and cycle life. This research could further direct future performance improvements through tuning the structure, controlling surface functional groups, optimizing electronic conductivity and doping with heteroatoms. Although this cathode requires pre-sodiated type anodes, we certainly believe that the favorable research progress in sodium metal anodes would enable the utilization of HGS cathodes towards high performance sodium metal battery applications.

Conflicts of interest

We do not declare any conflicts of interest.

Acknowledgements

This work was supported by the National Research Foundation of Korea (NRF) grant funded by the Korea Government (Ministry of Science, ICT & Future Planning) (No. 2016R1A4A1012224).

References

1 K. Kang, Y. S. Meng, J. Bréger, C. P. Grey and G. Ceder, *Science*, 2006, **311**, 977–980.
2 D. Larcher and J. M. Tarascon, *Nat. Chem.*, 2014, **7**, 19–29.
3 V. Palomares, M. Casas-Cabanas, E. Castillo-Martinez, M. H. Han and T. Rojo, *Energy Environ. Sci.*, 2013, **6**, 2312–2337.
4 J. Kim, D.-H. Seo, H. Kim, I. Park, J.-K. Yoo, S.-K. Jung, Y.-U. Park, W. A. Goddard Iii and K. Kang, *Energy Environ. Sci.*, 2015, **8**, 540–545.
5 M.-R. Gao, Y.-F. Xu, J. Jiang and S.-H. Yu, *Chem. Soc. Rev.*, 2013, **42**, 2986–3017.
6 R. Thangavel, A. Samuthira Pandian, H. V. Ramasamy and Y.-S. Lee, *ACS Appl. Mater. Interfaces*, 2017, **9**, 40187–40196.
7 H. Kim, Y.-U. Park, K.-Y. Park, H.-D. Lim, J. Hong and K. Kang, *Nano Energy*, 2014, **4**, 97–104.
8 R. Thangavel, B. Moorthy, D. K. Kim and Y.-S. Lee, *Adv. Energy Mater.*, 2017, 1602654.
9 H. Kim, G. Yoon, I. Park, J. Hong, K.-Y. Park, J. Kim, K.-S. Lee, N.-E. Sung, S. Lee and K. Kang, *Chem. Mater.*, 2016, **28**, 7241–7249.
10 R. Thangavel, K. Kaliyappan, D.-U. Kim, X. Sun and Y.-S. Lee, *Chem. Mater.*, 2017, **29**, 7122–7130.
11 C.-P. Yang, Y.-X. Yin, S.-F. Zhang, N.-W. Li and Y.-G. Guo, *Nat. Commun.*, 2015, **6**, 8058.
12 Y. Shao, J. Xiao, W. Wang, M. Engelhard, X. Chen, Z. Nie, M. Gu, L. V. Saraf, G. Exarhos, J.-G. Zhang and J. Liu, *Nano Lett.*, 2013, **13**, 3909–3914.
13 J. Zhang, W. Lv, Y. Tao, Y.-B. He, D.-W. Wang, C.-H. You, B. Li, F. Kang and Q.-H. Yang, *Energy Storage Materials*, 2015, **1**, 112–118.
14 G. Ali, A. Mehmood, H. Y. Ha, J. Kim and K. Y. Chung, *Sci. Rep.*, 2017, **7**, 40910.

15 L. Yu, L. Zhang, H. B. Wu and X. W. Lou, *Angew. Chem., Int. Ed.*, 2014, **53**, 3711–3714.
16 W. Zhang, X. Jiang, Y. Zhao, A. Carne-Sanchez, V. Malgras, J. Kim, J. H. Kim, S. Wang, J. Liu, J.-S. Jiang, Y. Yamauchi and M. Hu, *Chem. Sci.*, 2017, **8**, 3538–3546.
17 Y. Lu, L. Yu, M. Wu and X. W. Lou, *Adv. Mater.*, 2018, **30**, 1702875.
18 H. Cui, Z. Zhou and D. Jia, *Mater. Horiz.*, 2017, **4**, 7–19.
19 Y. Guo, J. Tang, J. Henzie, B. Jiang, H. Qian, Z. Wang, H. Tan, Y. Bando and Y. Yamauchi, *Mater. Horiz.*, 2017, **4**, 1171–1177.
20 R. Karthick, M. Brindha, M. Selvaraj and S. Ramu, *J. Colloid Interface Sci.*, 2013, **406**, 69–74.
21 M. Pumera, *Energy Environ. Sci.*, 2011, **4**, 668–674.
22 J. Liu, L. Zhang, H. B. Wu, J. Lin, Z. Shen and X. W. Lou, *Energy Environ. Sci.*, 2014, **7**, 3709–3719.
23 F. Cheng, J. Liang, Z. Tao and J. Chen, *Adv. Mater.*, 2011, **23**, 1695–1715.
24 W.-K. Shin, A. G. Kannan and D.-W. Kim, *ACS Appl. Mater. Interfaces*, 2015, **7**, 23700–23707.
25 R. Thangavel, A. G. Kannan, R. Ponraj, V. Thangavel, D.-W. Kim and Y.-S. Lee, *J. Power Sources*, 2018, **383**, 102–109.
26 S. W. Lee, N. Yabuuchi, B. M. Gallant, S. Chen, B.-S. Kim, P. T. Hammond and Y. Shao-Horn, *Nat. Nanotechnol.*, 2010, **5**, 531–537.
27 B. Z. Jang, C. Liu, D. Neff, Z. Yu, M. C. Wang, W. Xiong and A. Zhamu, *Nano Lett.*, 2011, **11**, 3785–3791.
28 S. Guo, H. Yu, P. Liu, Y. Ren, T. Zhang, M. Chen, M. Ishida and H. Zhou, *Energy Environ. Sci.*, 2015, **8**, 1237–1244.
29 C. Zhu, K. Song, P. A. van Aken, J. Maier and Y. Yu, *Nano Lett.*, 2014, **14**, 2175–2180.
30 Y. Zhong, M. Yang, X. Zhou and Z. Zhou, *Mater. Horiz.*, 2015, **2**, 553–566.
31 A. G. Kannan, A. Samuthirapandian and D.-W. Kim, *J. Power Sources*, 2017, **337**, 65–72.
32 D. Wu, X. Li, B. Xu, N. Twu, L. Liu and G. Ceder, *Energy Environ. Sci.*, 2015, **8**, 195–202.
33 K. Saravanan, C. W. Mason, A. Rudola, K. H. Wong and P. Balaya, *Adv. Mater. Energy*, 2013, **3**, 444–450.
34 Y.-U. Park, D.-H. Seo, H.-S. Kwon, B. Kim, J. Kim, H. Kim, I. Kim, H.-I. Yoo and K. Kang, *J. Am. Chem. Soc.*, 2013, **135**, 13870–13878.
35 X. Rui, W. Sun, C. Wu, Y. Yu and Q. Yan, *Adv. Mater.*, 2015, **27**, 6670–6676.
36 C. Zhu, C. Wu, C.-C. Chen, P. Kopold, P. A. van Aken, J. Maier and Y. Yu, *Chem. Mater.*, 2017, **29**, 5207–5215.
37 N. Yabuuchi, M. Kajiyama, J. Iwatate, H. Nishikawa, S. Hitomi, R. Okuyama, R. Usui, Y. Yamada and S. Komaba, *Nat. Mater.*, 2012, **11**, 512.
38 J. Qian, M. Zhou, Y. Cao, X. Ai and H. Yang, *Adv. Energy Mater.*, 2012, **2**, 410–414.
39 Y. Fang, L. Xiao, J. Qian, X. Ai, H. Yang and Y. Cao, *Nano Lett.*, 2014, **14**, 3539–3543.
40 V. Raju, J. Rains, C. Gates, W. Luo, X. Wang, W. F. Stickle, G. D. Stucky and X. Ji, *Nano Lett.*, 2014, **14**, 4119–4124.
41 H. Li, L. Peng, Y. Zhu, D. Chen, X. Zhang and G. Yu, *Energy Environ. Sci.*, 2016, **9**, 3399–3405.
42 H. V. Ramasamy, K. Kaliyappan, R. Thangavel, V. Aravindan, K. Kang, D. U. Kim, Y. Park, X. Sun and Y.-S. Lee, *J. Mater. Chem. A*, 2017, **5**, 8408–8415.
43 H. V. Ramasamy, K. Kaliyappan, R. Thangavel, W. M. Seong, K. Kang, Z. Chen and Y.-S. Lee, *J. Phys. Chem. Lett.*, 2017, **8**, 5021–5030.
44 Y. S. Yun, D. H. Kim, S. J. Hong, M. H. Park, Y. W. Park, B. H. Kim, H. J. Jin and K. Kang, *Nanoscale*, 2015, **7**, 15051–15058.
45 M. D. Slater, D. Kim, E. Lee and C. S. Johnson, *Adv. Funct. Mater.*, 2013, **23**, 947–958.
46 D. Lin, Y. Liu and Y. Cui, *Nat. Nanotechnol.*, 2017, **12**, 194.
47 Z. W. Seh, J. Sun, Y. Sun and Y. Cui, *ACS Cent. Sci.*, 2015, **1**, 449–455.
48 Y. Zhao, L. V. Goncharova, A. Lushington, Q. Sun, H. Yadegari, B. Wang, W. Xiao, R. Li and X. Sun, *Adv. Mater.*, 2017, **29**, 1606663.
49 A. P. Cohn, N. Muralidharan, R. Carter, K. Share and C. L. Pint, *Nano Lett.*, 2017, **17**, 1296–1301.
50 W. Luo, Y. Zhang, S. Xu, J. Dai, E. Hitz, Y. Li, C. Yang, C. Chen, B. Liu and L. Hu, *Nano Lett.*, 2017, **17**, 3792–3797.